A hierarchical application of the Minimum Current Corona

C. Beveridge and D.W. Longcope

Department of Physics, Montana State University, Bozeman MT59717-3840

ABSTRACT

We study the energy and helicity injected into the corona of a photospheric quadrupole by quasi-static motion. The minimum current corona (MCC) method provides a lower bound on coronal free energy by quantifying the coronal linkages between discrete photospheric source regions. A quadrupolar distribution can be modeled naturally with four photospheric sources. The coronal field connects the sources in four different ways (four domains) and includes one separator. The energy and helicity injection into this system were explored by Longcope and Magara (2004). The four-source configuration can be considered the most significant element of an MCC hierarchy whereby the continuous photospheric field is represented by an increasing number of discrete sources. The numbers of linkages and separators increase with the number of sources. This hierarchy asymptotically approaches a quasi-static MHD evolution line-tied to a continuous photospheric field. We demonstrate this hierarchy using an octopolar representation of the four-source experiment. We find that this refined representation has free energy and relative helicity significantly closer to those found in the line-tied numerical simulations. The better agreement occurs primarily because the refined system is able to represent self-helicities in the domains of the original system. Self-helicities are neglected by the MCC, and they are represented in the next level of the hierarchy as the mutual helicities between subdivisions.

1. Introduction

The magnetic field in the Sun's corona is both complicated and ever-changing. In the photosphere, flux elements ranging in size from intra-network regions ($\sim 10^{17}$Mx) to sunspots ($\sim 10^{21}$Mx) continually emerge, move around, fragment, cancel, coalesce and submerge. Since the coronal field is anchored to these *flux sources*, each of these activities can potentially lead to a large change in the corona.

The Minimum Current Corona (or MCC; Longcope 1996, 2001) was developed as a self-consistent, analytical model for the quasi-static evolution of the three-dimensional coronal field due to the movement of such photospheric flux sources. It simplifies the equation of ideal magnetohydrodynamics (MHD) by first assuming that coronal field lines are anchored in discrete *flux sources* separated by a contiguous region in which the normal magnetic field is zero.

As a result, each coronal field line can be assigned to one of a countable set of *flux domains* according to the source regions at each of its two footpoints. The interfaces between such domains are *separatrix* surfaces, which intersect along *separator* field lines. These surfaces and field lines comprise the magnetic field's *skeleton* (Priest, Bungey and Titov 1997; Longcope and Klapper 2002) and describe its connectivity.

MCC's second assumption is that the corona evolves quasi-statically through a series of force-free states, called *flux-constrained equilibria* or FCEs. An FCE is the field with the lowest magnetic energy which matches a prescribed photospheric boundary condition and distribution of domain fluxes. By constraining only domain fluxes the FCE minimisation permits footpoints to move *within* their photospheric flux source region. This is a notable contrast to *line-tying* which holds those footpoint locations fixed. The field resulting from line-tied minimisation is a general force-free equilibrium, while the FCE minimimum has current sheets along each separator but nowhere else (Longcope 2001).

The first assumption allows us to apply many of the techniques and equations of Magnetic Charge Topology (or MCT; see Longcope 1996; Longcope and Klapper 2002; Beveridge and Longcope 2005). In this paper, we will be assuming that the flux sources lie in a plane, which we call the *source plane.* Despite their name, the MCT equations do not require that the flux sources be represented as point charges, although point charges are the simplest flux arrangements satisfying MCC's first condition, and by far the easiest to calculate.

A *null point* exists where the magnetic field vanishes simultaneously in all three dimensions. A population of nulls must lie in the source plane; these are *photospheric nulls.* Nulls lying outside of the source plane are *coronal nulls.*

The field structure at a point $\mathbf{x}$ close to a null point at $\mathbf{x_n}$ is shown in Figure 1, and can be expressed as the first term of a Taylor expansion:

$$\mathbf{B}(\mathbf{x}-\mathbf{x_n}) = \mathbf{J}\cdot(\mathbf{x}-\mathbf{x_n}), \tag{1}$$

where $\mathbf{J}$ is the Jacobian matrix of the field (Parnell *et al.* 1996). Because $\nabla\cdot\mathbf{B} = \mathrm{tr}(\mathbf{J}) = 0$, the sum of $\mathbf{J}$'s eigenvalues vanishes; neglecting degenerate cases where one or more of the eigenvalues is zero, one eigenvalue (λ_1) is of opposite sign to the other two (λ_2 and λ_3). A *positive* null is one for which $\lambda_2 > 0$, and a *negative* null one where $\lambda_2 < 0$.

The eigenvector $\mathbf{e}_1$ associated with λ_1 defines two isolated field lines (beginning at

$\mathbf{x_n} \pm \delta\mathbf{e_1}$, for vanishingly small δ) called *spine* field lines. The sources at which the spine field lines end are the null's *spine sources.* If a photospheric null's spines lie in the source plane, the null is called *prone*; if they are directed out of the plane, the null is *upright.*

The remaining two eigenvectors ($\mathbf{e}_2$ and $\mathbf{e}_3$) define a *fan plane* $\mathbf{\Pi} = \mathbf{x_n} + \alpha\mathbf{e_1} + \beta\mathbf{e_2}$. Field lines beginning in the plane (for vanishingly small α and β) form a surface; if the null's spine sources are distinct, the surface is a *separatrix*, and it forms part of the boundary between two *flux domains*, contiguous volumes of field lines which end at the same sources.

If and only if a separatrix surface from a null n_a is partially bounded by a spine of a null of the opposite sign n_b, the separatrices of the two nulls intersect and a field line connects n_a to n_b (Beveridge 2003). This field line is a *separator*, and generally lies at the boundary of four distinct flux domains. It is a critical location for reconnection (Greene 1988; Lau and Finn 1990; Priest and Titov 1996; Galsgaard and Nordlund 1997); in the MCC model, current sheets are generally present on every separator.

The topology of a two-bipole system has been studied in many papers, including Sweet (1958); Gorbachev *et al.* (1988); Beveridge, Priest and Brown (2004) and, more recently, Longcope and Magara (2004), who made a detailed comparison between the results of analysing a simple two-bipole configuration with MCC and with an ideal, line-tied MHD simulation.

Beginning with two bipoles centred on the origin, and axes offset by an angle $\theta = 0.25\pi$ (see Figure 2), one of the bipoles was rotated until reaching $\theta = 0.50\pi$, while keeping constant the flux in each domain.

Comparing the flux in each domain between the potential state and the constrained state, they found time histories of separator current, helicity and free magnetic energy using

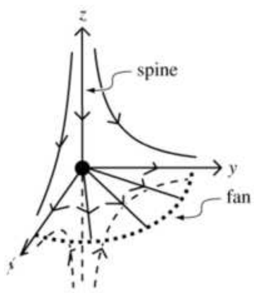

Fig. 1.— The three-dimensional field near a positive magnetic null point. Two isolated *spine* field lines approach the null, here from above and below. Nearby field lines spread out in a *fan* surface.

the MCC model and compared the results to an ideal, line-tied MHD simulation.

MCC successfully predicted the locations of the current sheets in the simulation; the separator current, however, was approximately a factor of four smaller in the MCC experiment. Free magnetic energy is again around a factor of four smaller[1]. The helicity, however, contains the most significant discrepancy. The exact helicity injection of the line-tied model is positive and peaks at $\theta = 0.5\pi$. However, the MCC helicity is negative and monotonically increases in magnitude.

The explanation for this difference is that each source in the rotating bipole rotates about its own centre. This internal rotation introduces a twisting of field lines in the line-tied model but does not in the MCC where internal footpoint motions are not prescribed. The field line twist takes the form of *self-helicity* and of distributed currents within the flux domains. Since the MCC does not prescribe internal footpoint motions both the self-helicty and distributed currents are absent. The MCC therefore contains only *mutual helicty* injected by the motion of the sources relative to one another. The mutal helicity is related to the separator currents, the only currents present in the MCC.

The present paper shows a means of reconciling these differences strictly within the MCC model by performing a hiererchical refinement of the problem. In the first level of refinement each of the four source regions is modeled with two point charges; the whole distribution consists of eight charges. Applying the MCC to this refined distribution permits the self-helicity from a given source region to be approximated as mutual helicity between its two charges. The energy and helicity predicted by the MCC given this distribution of charges match those of the line-tied experiment much better.

The paper is organized as follows. The next section presents the quadrupolar problem and its four-charge and eight-charge MCC representations. Section 3 proposes a hierarchical view of the minimum current corona, in which certain topological features are visible at different resolutions, and Section 4 gives their results. We conclude with a discussion of the project, its results and possible applications.

2. Configuration

Longcope and Magara considered the effects of rotating one bipolar source pair about another, both in a simple MCC representation ($C1$) and in a numerical, line-tied MHD simulation (which we label $C\infty$). We will refine the $C1$ model, as outlined previously, to

[1]Due to a programming error, that paper incorrectly finds the discrepancy to be an order of magnitude.

a more complicated MCC model with each of the four sources represented by two poles. We will designate these models $C2$ since they represent the second level in the hierarchical approximation of $C\infty$.

Following Longcope and Magara (2004), each source consists of a disk within which the vertical field is prescribed. The sources of the inner bipole (P1–N1) have centres separated by a distance ϵd, where ϵ is chosen to be 0.283. The outer, rotating bipole sources (P2–N2) have centres separated by d. The angle θ between the two bipole axes is allowed to vary between 0.25π and 0.75π.

The $C1$ approximation of this system is quite straighforward. Each source region (disk) is replaced by a single point charge with charge q_i, located at $(x, y, z) = (x_i, y_i, 0)$. In order to match the first two multipole moments of the source region (monopole and dipole) we take $q_i = \Phi_i/2\pi$, where Φ_i is the total vertical flux of the source region, and take (x_i, y_i) to be the centre of flux of the distribution within the plane (naturally $z_i = 0$ since all properties are measured at the photosphere, $z = 0$).

In the second level of the hierarchy, $C2$, each source region is represented by *two* charges of equal strength. The first two multipole moments are matched as long each has one-half the total charge and the midpoint lies at (x_i, y_i). Two charges are not sufficient to match all components of the third (quadrupole) moment so we settle for matching only the square of the radius of gyration

$$r_{\mathrm{g}}^2 \equiv \Phi_i^{-1} \int (x^2 + y^2) B_z(x, y, 0)\, dx\, dy$$

where the integral is over the source region of $C\infty$. Using the source distributions of Longcope and Magara (2004) fixes the separation between the charges at $2a = 0.212d$. We are free to choose arbitrarily the angle α of the speration line with the bipole axis. For the present investigation we consider two values: $\alpha = \pi/2$ (denoted case $C2_\perp$) and $\alpha = 0$ (denoted $C2_\parallel$).

In summary, the charges for the $C2$ are placed as follows:

Source	x/d	y/d	Φ/Φ_0
P1a	$-\epsilon$	a	0.5
P1b	$-\epsilon$	$-a$	0.5
N1a	ϵ	$-a$	-0.5
N1a	ϵ	a	-0.5
P2a	$\cos\theta + a\sin(\theta+\alpha)$	$\sin\theta - a\cos(\theta+\alpha)$	0.5
P2n	$\cos\theta - a\sin(\theta+\alpha)$	$\sin\theta + a\cos(\theta+\alpha)$	0.5
N2a	$-\cos\theta - a\sin(\theta+\alpha)$	$-\sin\theta + a\cos(\theta+\alpha)$	-0.5
N2b	$-\cos\theta + a\sin(\theta+\alpha)$	$-\sin\theta - a\cos(\theta+\alpha)$	-0.5

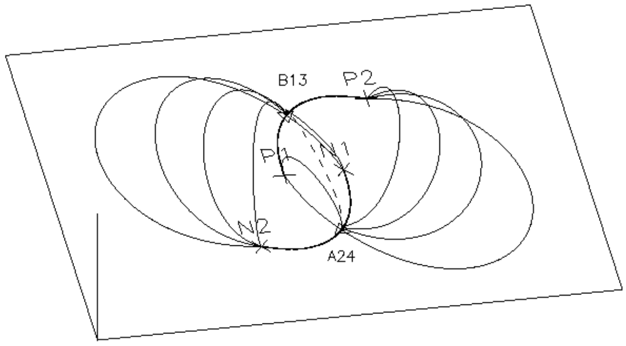

Fig. 2.— Original four-source topology, with $\theta = 0.25\pi$: intersecting state. The four sources are marked by crosses and the two null points by triangles. Separatrix field lines are thin solid lines, spine field lines thick solid lines and the separator the dashed line.

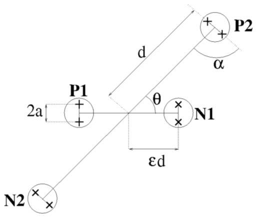

Fig. 3.— The parameters of a $C2$ configuration. Two inner sources of opposite sign have their centres on the x-axis. Two outer sources have their centres separated by a distance d on a line passing through the origin and forming an angle θ with the x-axis. Each source consists of two poles of strength $0.5\Phi_0$, placed a distance a from the source centre on a line forming an angle α with the bipole axis.

In both cases $C2_\perp$ and $C2_\parallel$ the dipole is rotated by varying θ from 0.25π to 0.75π, although Longcope and Magara (2004) considered a rotation over only half this range. While the dipole rotates the value of α is held fixed causing the two charges within a source to rotate about one another. It is this relative rotation which will inject helicty into the flux anchored within a source region. This self-helicity injection was absent in the $C1$ model and we wish to investigate how its approximate inclusion helps.

3. Hierarchy

The refined models, $C2_\perp$ and $C2_\parallel$, have more point charges so they will naturally have more topological features, such as flux domains, separators, and null points. To compare models of increasing complexity it is helpful to construct a hierarchy of MCC concepts. This will enable us to examine a topology at several resolutions: a low-resolution representation will help us understand the physics conceptually, while a higher-resolution will enable a more accurate computation of results.

The lowest-resolution picture, $C1$, is the bottom of the hierarchy so we designate each of its charges as a *level-1* source. They are labeled $P1$, $P2$, $N1$ and $N2$. The charges at the next level of the hierarchy, $C2$, are called *level-2* sources. Each can be traced up one level to a unique level-1 source, which we call its *parent* source. We use a labelling which indicates the parentage of each level-2 source; for example, the children of level-1 source $P1$ are $P1a$, $P1b$.

All domains at a given level are designated by the level of that model. A level-2 domain is one that connects two level-2 sources. It has a *parent domain* at level-1 connecting the parents of its two sources. Thus each level-2 domain has a unique level-1 parent.[2]

We begin with a topological analysis of the potential fields from models at each hierarchical level. Systematic analysis of this type begins with an identification and classification of all the magnetic null points in the field. The two spine field line from a given null point are followed to their ends at magnetic charges called the *spine sources*. A null point is given a level index according to the parentage of its two spine sources. If both spines end at the same spine source it is called *homospinal*, its fan is not a genuine element of the skeleton (Longcope and Klapper 2002) and it is therefore not assigned a level index. The index of a

[2]It is theoretically possible for a level-2 domain to connect sources whose parents were *not* connected in the level-1 model. We neglect these parent-less domains (orphans) for now since $C1$ contains all possible interconnections (i.e. all possible parents exist).

heterospinal null designates the level at which the parentage of the spine sources first differs. Thus a null point in $C2$ whose spine sources have the same level-1 parent is a level-2 null point, while one whose spine sources have different level-1 parents is a level-1 null point.

A magnetic separator is the intersection of fan surfaces from two null points of opposing sign. The separator is assigned a pair of level-indices according to the levels of the nulls it connects. A level-1/2 separator connects a level-1 null to a level-2 null.

In the present example the field from $C1$ contains two prone null points, one of either sign, and a single separator connecting them. Since these features appear at the lowest level the null points and the four flux domains are all designated level-1 and the separator is level-1/1.

The topology at the next level depends to some extent on values of α and θ. Footprints for $\theta = 0.25\pi$ (the initial state) are shown in the left column of Figure 4 for both $C2_\perp$ (top) and $C2_\parallel$ (bottom). In both cases there are two level-1 nulls and four level-2 nulls. The latter are easily identified since they lie immediately between two sources from the same level-1 parent. The two level-1 nulls have obvious counterparts in $C1$. Since the quadrupole moments of a source are different in each model, the null point locations differ slightly between them.

The right panels of Figure 4 show the separators for $C2_\perp$ (top) and $C2_\parallel$. In each there is one at level-1/1 (solid), four at 1/2 (dashed) and two at 2/2 (dotted). The level-1/1 separator in each is the counterpart of the separator in $C1$. The level-1/2 separators in each of the models can be associated with one another according to the nulls they each connect. In each case there is a pair of "inner" separators, connecting level-2 nulls from the small dipole to level-1 nulls, and pair of "outer" separators connecting level-2 nulls from the outer dipole to the level-1 nulls. On the other hand, the level-2/2 separators in $C2_\perp$ connect different nulls than the ones in $C2_\parallel$. This will prove to be a major source of discrepancies between the versions of the $C2$ models.

It is possible, in principle, for the topology of a given model to change through bifurcation as the bipolar angle θ is varied. Remarkably such bifucations do not occur in either model over the range we consider: $0.25\pi \leq \theta \leq 0.75\pi$. This is fortunate as a practical implementation of the MCC is only possible for sufficiently small departures from the potential configuration. A bifurcation by definition causes significant topological changes and the physical quantities are likely to undergo abrupt changes at these locations.

According to a relation established by Beveridge and Longcope (2005), there are:

$$D = X + S - N_c - 1 \tag{2}$$

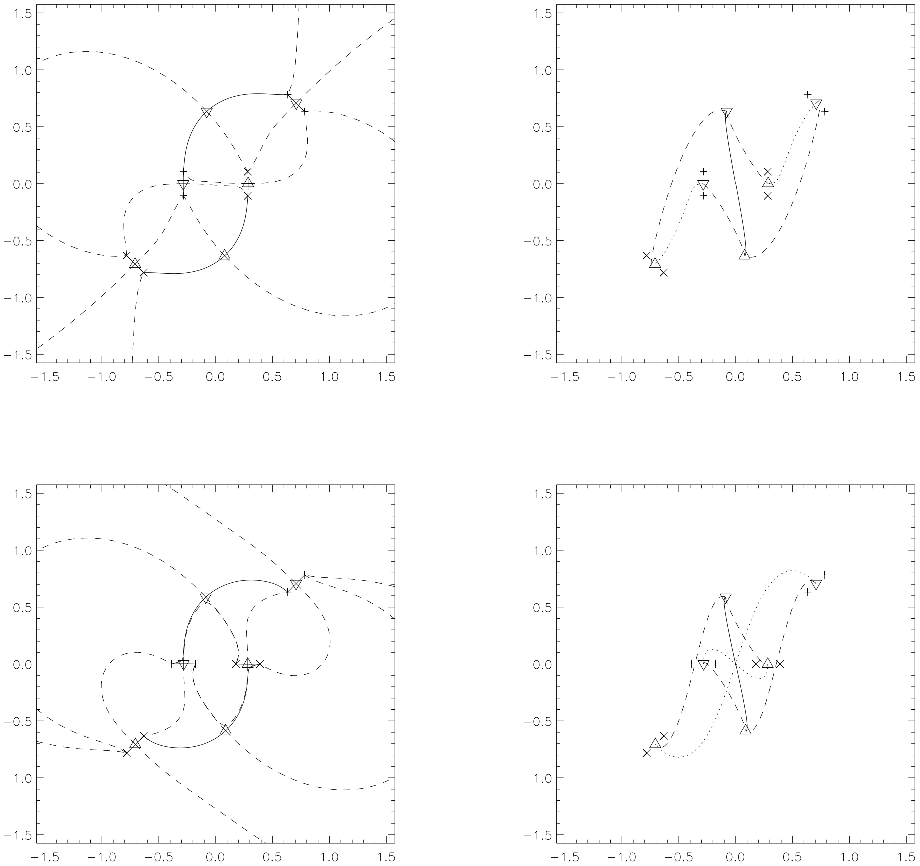

Fig. 4.— *Left:* Footprints of the $C2$ configurations: *above*, $C2_{\perp}$ and *below*, $C2_{\parallel}$. Nulls are denoted by triangles, sources by crosses, spine field lines by solid lines and separatrix traces by dashed lines. There two level-1 nulls which exist in $C1$ and both $C2$ configurations. In addition, four level-2 nulls are present. Twelve photospheric flux domains can be counted in this figure; two coronal domains are also present. *Right:* Separators: *above*, for $C2_{\perp}$ and *below*, for $C2_{\parallel}$. The level-1/1 separator is denoted by a solid line, the level-1/2 separators by dashed lines and level-2/2 separators by dotted lines. Note that the level-2/2 separators connect different nulls in the two setups.

flux domains (D), where X is the number of separators (here, 7), S the number of sources (8) and N_c the number of coronal nulls (none); thus $D = 14$. There are two separator circuits, implying two coronal domains (Longcope and Klapper 2002).

All flux domains are level-2 domains and each can be identified with a level-1 parent. The level-2 domains can be seen as subdivisions of the level-1 domains. The domain graphs in Figure 5 are schematic depictions of all level-1 domains (top) and level-2 domains (bottom). The layout suggests how the level-1 domains are differently subdivided in $C2_\perp$ and $C2_\parallel$. For example, level-1 domains $P1$–$N2$ and $P2$–$N1$ (diagonal lines) are subdivided into four domains each by $C2_\perp$ (lower left) and into three domains each by $C2_\parallel$ (lower right).

The differing subdivision is a direct consequence of the different level-2/2 separators. By definition, each level-2 null point has spine sources with the same level-1 parent. Each positive (negative) level-2 null point may therefore be associated with a single positive (negative) level-1 *source*. By extension the level-2/2 separator connecting the nulls may be associated with the level-1 domain connecting the associated sources. The level-2/2 separators in $C2_\perp$ are thereby associated with level-1 domains $P1$–$N2$ and $P2$–$N1$, while those in $C2_\parallel$ are associated with $P1$–$N1$ and $P2$–$N2$. There is a symmetry between the first pair, which interconnect the small and large dipoles, so we can expect the two level-2/2 separators in $C2_\perp$ to have identical properties. This will not be the case in $C2_\parallel$ where the level-2/2 separators are associated with dissimilar domains: one is entirely in the large bipole while the other is entirely in the small bipole.

According to Longcope and Klapper (2002) there is a one-to-one correspondence between separators and circuits in the domain graphs (sets of domains which can be followed in a closed sequence). Such a circuit will exist here whenever a level-1 domain is subdivided into four level-2 domains interlinking all four level-2 children. Indeed this circuit exists entirely within the level-1 parent domain so the associated separator must be associated with that same domain. This explains why $C2_\perp$ subdivides domains $P1$–$N2$ and $P2$–$N1$ into four domains each while it divides $P1$–$N1$ and $P2$–$N2$ into *three* each: because it has level-2/2 separators associated with the first two and not with the last two.

Different values of α would yield still different topologies. Some of these have more level-2/2 separators and subdivide each level-1 domain into four (or more) level-2 domains. In a brief survey of alternative cases we have been unable to find one which remains bifurcation-free for any significant change of θ. Because they are quite robust and serve to illustrate the various possibilities we continue to consider only the two cases $C2_\perp$ and $C2_\parallel$. The assortment of topological features in each are summarized in Table 1.

In theory, this type of analysis could be perfomed on succesive levels in the hierarchy.

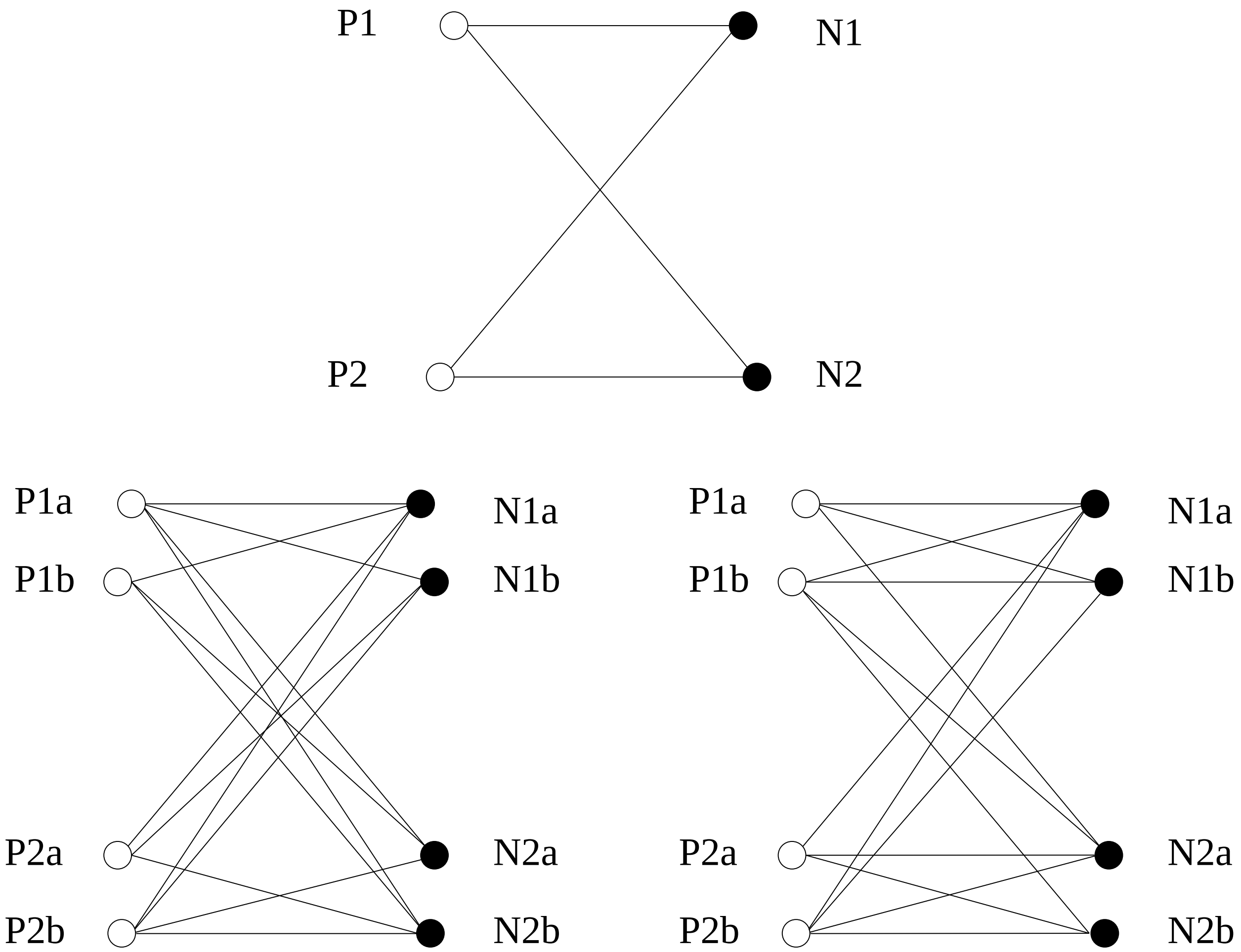

Fig. 5.— Domain graphs showing the flux domains in $C1$ (top), $C2_{\perp}$ (lower left) and $C2_{\parallel}$ (lower right).

Feature	$C1$	$C2_{\perp}$	$C2_{\parallel}$
Sources	4	8	8
Nulls	2	6	6
Coronal nulls	0	0	0
Separators	1	7	7
Domains	4	14	14
Coronal domains	0	2	2

Table 1: Numbers of categorised skeleton elements in the three configurations considered. All three satisfy the Beveridge-Longcope equation $D = X + S - N_c - 1$. Although the element counts are identical for the $C2$ cases, the topologies are geometrically distinct.

As each source is further sub-divided it will be possible to match an increasing number of multi-pole moments from the original source regions. In the limit of ∞ charges all multi-pole moments are matched, which is equivalent to matching the magnetic field distribution $B_z(x, y)$ at every point. This case, $C\infty$ corresponds to the line-tied case studied by Longcope and Magara (2004). Each field line would constitute its own flux domain, and there would be an infinite number of null points and separators. The MCC would therefore dictate an infinite number of constraints, one for each separator, which must match in some sense the infinity of constraints imposed by line-tying.

4. Results

Each of the models described above, $C1$, $C2_\perp$ and $C2_\parallel$ is time-evolved by varying θ from the initial value, $\theta_0 = 0.25\pi$ up to 0.75π. The system is taken to be in a potential state initially, and changed continuously according to the MCC. To do this we must find the flux constrained equilibria for each θ having the same domain fluxes it had for θ_0.

According to the MCC theory (Longcope and Klapper 2002) these flux constraints are equivalent to constraining the flux Ψ_σ through each of the separators to have the same value it had for the potential field at θ_0: namely $\Psi_\sigma^{(v)}(\theta_0)$. The fluxes for a potential field, $\Psi_\sigma^{(v)}(\theta)$, through each separator are found for each value of θ. The MCC then requires that currents contribute an additional flux, $\Delta\Psi_\sigma$, through each separator. These can be decomposed into self-inductive and mutual-inductive contributions

$$\Delta\Psi_\sigma = \Psi_\sigma^{(v)}(\theta_0) - \Psi_\sigma^{(v)}(\theta) = \Delta\Psi_\sigma^{(\mathrm{self})} + \Delta\Psi_\sigma^{(\mathrm{mut})} \quad . \tag{3}$$

For sufficiently small departures from a potential field both contributions can be approximated using the separator currents, I_σ, and properties of the separators in the potential field from the present boundary. The self-inductive contribution is

$$\Delta\Psi_\sigma^{(\mathrm{self})} = \frac{L_\sigma I_\sigma}{4\pi} \ln\left(\frac{eI_\sigma^*}{|I_\sigma|}\right), \tag{4}$$

where $e = 2.718$ is the base of the natural logarithm, L_σ is the total length of the separator and I_σ^* is a fiducial current proportional to the perpendicular magntic shear of the potential field averaged along the separator field line (Longcope and Magara 2004).[3] The mutual

[3]In this experiment we follow Longcope and Magara's convention of using rationalised cgs units. These can be converted to cgs units proper by multiplying all currents by $c/4\pi$ or to mks units by dividing currents by μ_0.

inductive contribution is

$$\Delta\Psi_\sigma^{(\mathrm{mut})} = \sum_{\mu\neq\sigma} M_{\mu\sigma} I_\mu, \tag{5}$$

where $M_{\mu\sigma}$ is the mutual inductance between separators μ and σ found by the classic Neumann formula (Jackson 1975).

Using these forms in the full expression (3) gives a non-linear set of coupled equations for the unknown currents, I_σ, in terms of the known flux differences, $\Delta\Psi_\sigma$. We solve the equations numerically using Newton-Raphson iterations begining with the solution to the uncoupled non-linear equations arising from neglecting the mutual contributions: $\Delta\Psi_\sigma^{(\mathrm{v})} = \Delta\Psi_\sigma^{(\mathrm{self})}(I_\sigma)$.

The current on the level-1/1 separator, shown in Figure 6, is roughly comparable in all three of the models. The current flows in the direction opposite to the magnetic field, so it is negative by convention. The different models approximate the sources with charge distributions with the same monopole and dipole terms but differing in all higher multipole terms. The refinements of $C2$ leads to a more accurate approximation of the $C\infty$ field by matching more terms in the multipole expansion. Since the separator lies far from the sources, however, this increased accuracy has little effect (see Figure 7).

The other separator currents (see Figure 8) all begin in the same direction as the magnetic field (they are positive); however, as the rotation continues, each of the currents reaches a peak value and then falls. In many cases the current reverses direction. The level-1/2 separators (dashed curves) carry relatively little current at any point. Since they are symmetric, each of the inner separators carries the same current (lower dashed curve). The same is true of the outer separators (upper dashed curve). It is noteworthy that the current on each type does not differ significantly between $C2_\perp$ and $C2_\parallel$

The level-2/2 separator currents differ significantly between the two models. In model $C2_\perp$ the two separators are symmetric and therefore carry the same current. These separators fall in the level-1 domains $P1$–$N2$ and $P2$–$N1$ as discussed in the previous section. Each of these domains is anchored at one end to a rotating source ($P1$ or $N1$) and at the other to a static source ($P2$ and $N2$). The ends of the domain are thus differentially twisted, in the sense to create current parallel to the field ($I > 0$). The line-tied simulations did, in fact, exhibit positive current distributed within each of these domains (Longcope and Magara 2004). In the $C1$ model, however, the internal motion of the sources is neglected so no such current occurs. It seems that the level-2/2 separators in model $C2_\perp$ are capable of responding to the differential rotation of their associated level-1 domains.

The level-2/2 separators in $C2_\parallel$ are not symmetric so each carries a different current. One separator (lower curve) is associated with level-1 domain $P2$–$N2$ whose footpoints never

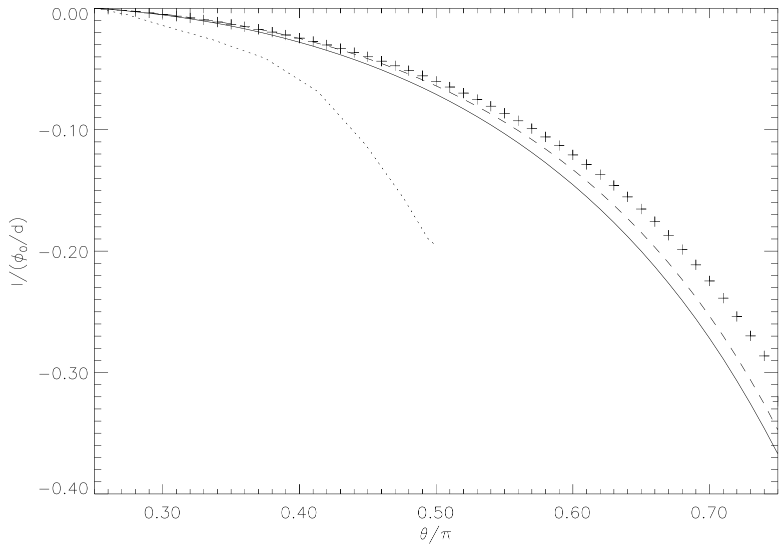

Fig. 6.— Level-1/1 separator currents. Solid line: Current on $C2_{\perp}$'s level-1/1 separator. Crosses: current on $C2_{\parallel}$'s level-1/1 separator. Dashed line: Current on $C1$'s separator. Dotted line: Current on $C\infty$'s separator.

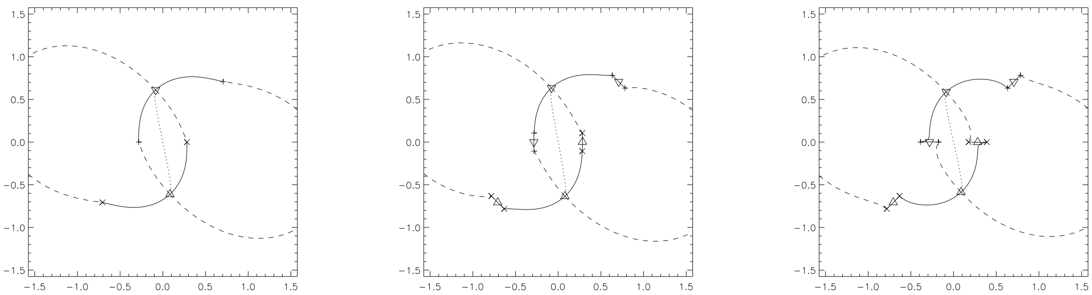

Fig. 7.— Level-1 footprints of $C1$ (left), $C2_{\perp}$ (centre) and $C2_{\parallel}$ (right). Each footprint consists of the fan traces (dashed) and spines (solid) of only the level-1 nulls. The spines of the level-2 nulls are also shown for clarity.

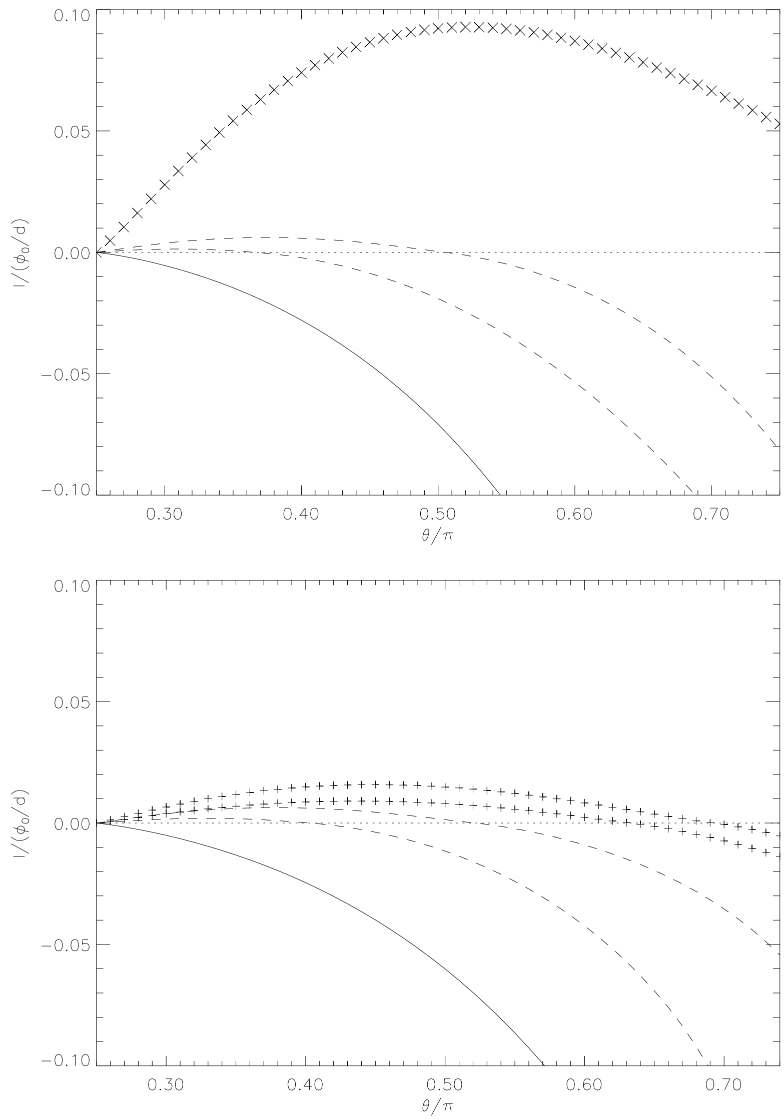

Fig. 8.— Separator currents for $C2_\perp$ (*top*) and $C2_\parallel$ (*bottom*). Solid line: level-1/1 separator current; dashed line: level-1/2 separator currents; crosses: level-2/2 separator current(s). Note that the level-2/2 current is much stronger in $C2_\perp$ than in $C2_\parallel$. The remaining currents are similar in the two configurations.

move. The other domain is associated with level-1 domain $P1$–$N1$ whose footpoints rotate rigidly about each other and thus do not rotate differentially. Without differential twisting in either domain we expect little current injection. In fact, the current on neither of level-2/2 separators is very large.

4.1. Helicity

The twisting of field lines is quantified by the relative helicity of the magnetic field (Berger and Field 1984; Finn and Antonsen 1985),

$$H_R = \int_{z>0} (\mathbf{B} - \mathbf{B_p}) \cdot (\mathbf{A} + \mathbf{A_p}) \mathrm{d}\mathbf{x}, \tag{6}$$

where $\mathbf{B_p}$ is the potential field with the same charge setup, and $\mathbf{A}$ and $\mathbf{A_p}$ are vector potentials for $\mathbf{B}$ and $\mathbf{B_p}$, respectively. When the coronal evolves ideally subject to a photospheric velocity field $\mathbf{v}(x, y)$ the helicity injection is given by

$$\frac{dH_R}{dt} = -2 \int_{z=0} (\mathbf{A}_p \cdot \mathbf{v}) B_z \, dx \, dy. \tag{7}$$

Expression (7) can be applied to the line-tied model, $C\infty$, since the photospheric motion is a known, prescribed function. Doing so shows that the combination of circular motion and internal rotation by $P1$ and $N1$ creates positive helicty, indicating a right-handed sense of twist (see Figure 9). The helicity increases up to $\theta \simeq \pi/2$, and then begins to decline.

The MCC does not prescribe the the footpoint motions *within* sources, so this expression is not applicable to its evolution. Instead one must use the magnetic field in (6). Introducing an auxiliary field $\mathbf{Z}$ such that $\nabla \times \mathbf{Z} = \mathbf{A}$ for $\mathbf{A}$ in the Coulomb gauge, we can integrate by parts to obtain (Longcope and Magara 2004):

$$H_R^{(FCE)} = \int_{z>0} \mathbf{J} \cdot (\mathbf{Z} + \mathbf{Z_p}) \mathrm{d}\mathbf{x} \simeq \sum_{\sigma} 2 I_{\sigma} \int_{\sigma} \mathbf{Z_p} \cdot \mathrm{d}\mathbf{l}. \tag{8}$$

This may be used to find the helicities in models $C1$ and $C2$ using the currents found on each separator.

The helicity in $C1$ is negative in notable contrast to $C\infty$. Negative helicity is consistent with the relative motions of the source centroids (Longcope and Magara 2004) wrapping the domains around each other in a left-handed sense. The relative twist of two domains about one another is called *mutual helicity*. The full helicity is positive due to the *self-helicity* from

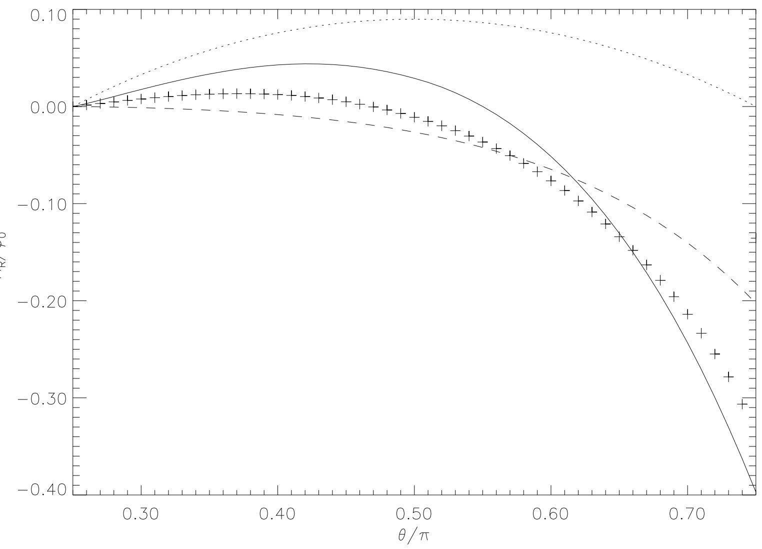

Fig. 9.— Comparison of total helicity in the four cases considered. Solid line: total helicity in $C2_\perp$. Crosses: total helicity in $C2_\parallel$. Dashed line: total helicity in $C1$. Dotted line: total helicity in $C\infty$.

differential twist within each domain. Since this differential twisting is not accounted for in $C1$ only the negative mututal helicity is present.

The $C2$ models approximate the self-helicity in level-1 domains as mutual helicity between level-2 subdivisions. The curves in Figure 9 show that this succeeds to a significant extent. The $C2_\perp$ case (solid line) is the best approximation since it subdivides each of the most twisted domains into four: $P1$–$N2$ and $P2$–$N1$. The resulting helicity peaks at $\theta = 0.42\pi$ at approximately half the value of the $C\infty$. Model $C2_\parallel$ also has sufficient self helicity to overwhelm the negative mutual helicity. Its level-2/2 separators are associated with domains $P1$–$N1$ and $P2$–$N2$. Since these domains are not differentially twisted it is not surprising that the helicity of $C2_\parallel$ is much smaller than than of $C2_\perp$.

4.2. Free energy

The magnetic energy in the MCC is minimised subject to constraints and is therefore higher than the unconstrained minimum: the energy of the potential field. The excess energy demanded by the constraints is called the *free energy* and is denoted ΔW. As with the current, the free energy combines contributions due to self-inductance and a mutual inductance (Longcope 2001)

$$\Delta W = \Delta W^{(\mathrm{self})} + \Delta W^{(\mathrm{mut})}, \tag{9}$$

where

$$\Delta W^{(\mathrm{self})} = \sum_\sigma \frac{L_\sigma I_\sigma^2}{32\pi^2} \ln\left(\frac{e^{0.5} I_\sigma^*}{|I_\sigma|}\right) \tag{10}$$

$$\Delta W^{(\mathrm{mut})} = \sum_\sigma \sum_{\mu\neq\sigma} \frac{M_{\mu\sigma} I_\mu I_\sigma}{16\pi}. \tag{11}$$

Figure 10 shows the energies of the various models. In order to see the effect of the higher level separators we also perform calculations using $C2$ models in which constraints are applied only on the level-1/1 separators. These have the same boundary conditions as, but impose fewer constraints than, the full MCC. They therefore have strictly lower energies than the corresponding full MCC curve.

It is not easy to compare these results to a quasi-static $C\infty$ energy. Longcope and Magara (2004) performed a time-dependent numerical simulation to approximate the line-tied case. Unfortunately the dynamical result departs from equilibrium and this departure introduces significant extra energy. To find a better approximation Longcope and Magara

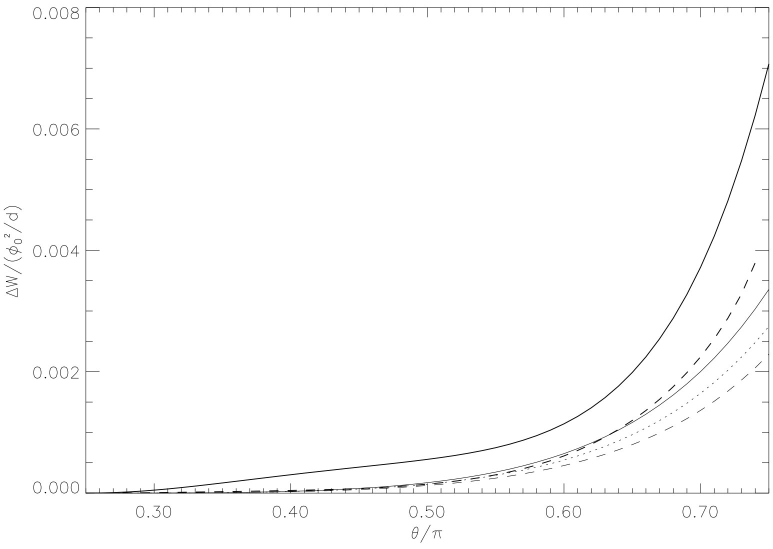

Fig. 10.— Free magnetic energy in $C1$ (dotted line) and $C2$. The thicker lines represent energies for $C2_\perp$ and the thinner ones $C2_\parallel$. Solid lines are the free energy holding the flux through each separator constant; dashed lines the energy from a constraint only on the level-1/1 separator.

derived a lower bound on the free energy consisting of a contribution due to the configuration's self-helicity (the rotation of each source) and its mutual helicity (the tangling of level-1 flux domains). We use the mutual helicity of a $C2$ configuration as our best estimate of that in $C\infty$. As this helicity is effectively unchanged from $C1$, and the self-helicity of $C\infty$ remains unchanged, we conclude that we cannot improve on their $C\infty$ energy estimate.

We find that the energy for $C2_\perp$ is roughly a factor of four greater than that available from the true energy of $C1$; our result is approximately 75% of the lower bound for $C\infty$. However, the energy for $C2_\parallel$ is only marginally higher than that for $C1$.

5. Discussion

In this paper, we have studied the effects of rotating a complex bipolar system around another ($C2$), in comparison to a simpler four-pole representation ($C1$) and a numerical, line-tied version ($C\infty$), both of which were considered by Longcope and Magara (2004). Our eight-pole system agrees far more closely in its results for free magnetic energy and helicity to the line-tied model than does $C1$.

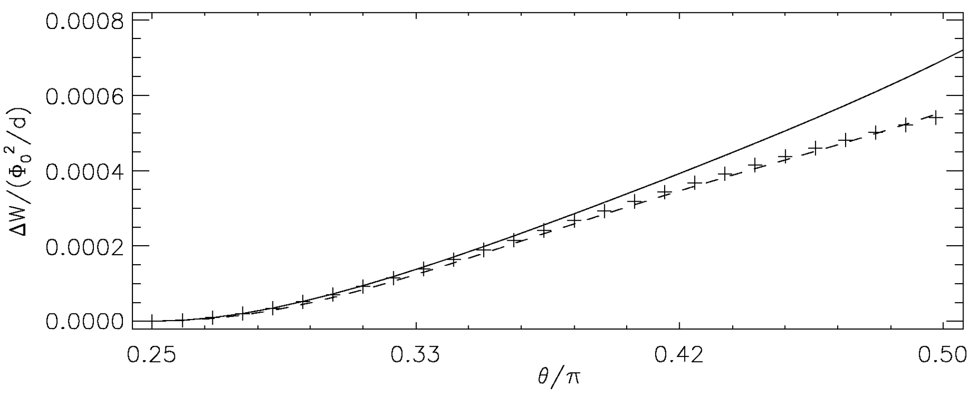

Fig. 11.— Magnetic energy in $C2$ and $C\infty$. Solid line: Longcope and Magara's estimated lower bound on $C\infty$'s energy. Crosses: Lower bound on C_∞'s energy from self-helicity. Dashed line: Free magnetic energy of $C2_\perp$. The close correlation of these last two is apparently coincidental.

Because the eight-pole configuration allows a source region to rotate about its centre, extra self-helicity is injected into the system. As the poles rotate anticlockwise, this injection is positive. In combination with the negative mutual helicity, this causes the total helicity to rise in the early stages before peaking and falling back to zero and below. This qualitatively mimics the behaviour of the exact total helicity calculated by Longcope and Magara, which peaks at $\theta = 0.5\pi$. Our peak value is, however, around half of theirs.

The free magnetic energy in the $C1$ configuration is found to be around 25% of the theoretical minimum of $C\infty$ given by Longcope and Magara (2004). The extra helicity injected into the $C2_\perp$ configuration increases the free energy threefold, to around 75% of the $C\infty$ limit. The $C2_\parallel$ configuration, however, does not significantly increase the free energy.

A reason for this discrepancy may be the arrangements of separators inside level-1 flux domains. In the $C2_\parallel$ configuration, both of the level-2/2 separators lie within level-1 domains connecting the two poles of a single bipole. Since these domains are not differentially rotated with respect to each other, little helicity is injected into the separator and correspondingly little energy is stored compared to Longcope and Magara's $C1$ configuration. In contrast, the level-2/2 separators of the $C2_\perp$ configuration both lie within level-1 domains, the end points of which are in different bipoles, and which undergo differential rotation. This forces a greater helicity injection than in the $C2_\parallel$ set-up and hence a greater energy storage. The difference in helicity injection can be seen clearly in Figure 9.

This application of a hierarchical MCC model to a relatively complex configuration has yielded encouraging results. With the advent of automatic methods for modelling MDI flux patches as collections of charges and improved algorithms for finding domain fluxes, we hope to extend this work to more complicated and more realistic configurations.

Acknowledgements

This material is based upon work supported partially by the National Science Foundation under grant ATM-0416340 and by NASA under grant NAG5-10489.

REFERENCES

Berger, M.A. and Field, G.B.: 1984, *J. Fluid Mech.*, **147**, 133.

Beveridge, C.: 2003, Ph.D. Thesis, University of St. Andrews.

Beveridge, C. and Longcope, D.W.: 2005, *Solar Physics*, accepted.

Finn, J., and Antonsen, J.T.M.: 1985, *Comments Plasma Phys. Controlled Fusion*, **9**, 111.

Beveridge, C., Priest, E.R. and Brown, D.S.: 2004, *Geophys. Astrophys. Fluid Dynamics*, **98**, 429.

Galsgaard, K. and Nordlund, Å: 1997, *J. Geophys. Res.*, **102**, 231.

Greene J.M,: 1988, *J. Geophys. Res.*, **93**, 8583.

Gorbachev, V.S., Kel'ner, S.R., Somov, B.V., and Schverts, A.S.: 1988, *Soviet Astron.*, **32**, 308.

Jackson, J.D.: 1975, *Classical Electrodynamics*, Wiley, New York.

Lau, Y.-T. and Finn, J.M.: 1990, *Astrophys. J.*, **366**, 577.

Longcope, D.W.: 1996, *Solar Phys*, **169**, 91.

Longcope, D.W.: 2001, *Phys. Plasmas*, **8**, 5277.

Longcope, D.W. and Klapper, I., 2002: *Astrophys. J.*, **579**, 468.

Longcope, D.W. and Magara, T., 2004:

Parnell, C.E., Smith, J.M., Neukirch, T. and Priest, E.R.: 1996, *Phys. Plasmas*, **3**, 759.

Priest, E.R., Bungey, T. and Titov, V.S., 1997: *Geophys. Astrophys. Fluid Dynamics*, **84**, 127.

Priest, E.R. and Titov, V.S.: 1996, *Phil. Trans. R. Soc. London*, **A354**, 2951.

Sweet, P.A.: 1958, *Nuovo Cimento*, **8**, 188.
